Magnetic Ordering in Rare Earth Metal Dysprosium Revealed by Neutron Diffraction Studies in a Large-Volume Diamond Anvil Cell

Christopher Perreault and Yogesh K. Vohra*

Department of Physics, University of Alabama at Birmingham, Birmingham, Alabama 35294, USA

Antonio M. dos Santos, Jamie J. Molaison, Reinhard Boehler

Neutron Scattering Division, Oak Ridge National Lab, Oak Ridge, Tennessee 37831, USA

* Correspondence to [ykvohra@uab.edu]

ABSTRACT

A high-pressure low-temperature neutron diffraction study has been carried out on rare earth metal Dysprosium (Dy) to 10.8 GPa and 8 K in a large-volume diamond anvil cell using a spallation neutron source. Dy crystallizes in an ambient pressure hexagonal close packed phase and forms an incommensurate helical antiferromagnetic phase, marked by the appearance of superlattice magnetic peaks below 176 K with a turn-angle between the hexagonal layers that increases both with increasing temperature and pressure. The ferromagnetic transition below 87 K is marked by an increase in intensity of nuclear peaks with disappearance of magnetic superlattice reflections. Dy transforms to an alpha-Samarium (*α-Sm*) phase at 7 GPa and only ferromagnetic ordering is observed for this high pressure phase. The ferromagnetic transition is observed at 59 K in the *α-Sm* phase at 10.8 GPa in close agreement with the magnetic ordering temperature obtained from electrical transport measurements. In the entire pressure-temperature range of this study, Dy shows a negative thermal expansion coefficient of as much as -2.5 % in the magnetically ordered phases between 200 K and 8 K.

I. INTRODUCTION

Rare earth elements are of particular interest from a fundamental perspective due to their complex electronic structure arising from the sequential filling of the *4f* shell which leads to rich phase diagrams and unique properties [1]. The similarity of high-pressure behavior of *4f* rare earth metals to the *5f* actinide metals under compression make these studies particularly attractive as has been noted in case of actinide metal thorium under high pressure and its similarity with rare earth metal cerium [2]. With one of the highest intrinsic magnetic moment of 10.6 Bohr magneton (μ_B) among the heavy rare-earth elements, dysprosium (Dy) exhibits a rich magnetic phase diagram under high pressure and low temperature conditions. The recent innovations in measurements of magnetic ordering temperature in rare earth metals by electrical transport techniques have revealed complex magnetic behavior in Dy and have extended electrical resistivity measurements to above 100 GPa [3, 4]. The magnetic transitions detected by electrical resistivity measurements have been validated by the direct observation of magnetic structures by neutron diffraction studies at high pressures and low temperatures [5, 6]. Recently, the equation of state of metallic dysprosium has been measured up to 35 GPa and low temperatures, between 200 K and 7 K, using angle dispersive x-ray diffraction at a synchrotron source [7]. These measurements shows that Dy has anomalous thermal expansion in the magnetically ordered state and normal thermal expansion in the paramagnetic state for all the three known high pressure phases (*hcp*, *α-Sm*, and *dhcp*) observed within the measured pressure range. However, owing to the inability to probe the magnetic structure using x-ray diffraction, a complete picture cannot be obtained without companion neutron diffraction measurements at similar pressure and temperature ranges. Furthermore, owing to the traditional pressure and temperature limitations of high pressure neutron scattering, the determination of the magnetic structure of the high pressure phases is still lacking.

At ambient pressure, the paramagnetic (PM) to helical antiferromagnetic (AFM) transition at T_N = 176 K and AFM to ferromagnetic (FM) transition at T_C = 87 K are well documented [8]. In the helical structure the magnetization is always in the basal plane perpendicular to the c-axis but changes in direction from one hexagonal close-packed plane to the next with a turn angle (θ) that is temperature and pressure dependent. The propagation or wave vector **q** is defined in terms of turn angle and is given by (0, 0, θ). This turn-angle has been measured at ambient pressure by neutron diffraction studies and increases almost linearly with temperature from 27 ^{o} at 87 K to 43

^{o} per layer at 176 K [10]. The magnetic ordering transition temperature measured by electrical resistivity technique in Dy shows a decrease with increasing pressure in the *hcp*-phase followed by a discontinuous drop on transition to the *α-Sm* phase at 7 GPa (Fig. 1) [3]. The magnetic ordering transition then undergoes a minimum and then increases with further increase in pressure in the *dhcp*-phase to 35 GPa [3]. Dy also shows unconventional magnetic state under ultra-high pressures as the magnetic ordering temperature increases rapidly above 70 GPa and attains a value greater than ambient temperature of 300 K at pressures above 107 GPa [4]. The results of electrical transport measurements described above only indicate to the possibility of magnetic order, however, no direct information is currently available on the type of magnetic order in Dy at high pressures. We have performed neutron scattering experiments on Dy at high-pressures and low-temperatures and characterized both the AFM and FM ordering in the ambient pressure *hcp* and high pressure *α-Sm* phase. In addition, direct experimental evidence is presented for the negative thermal expansion in the magnetically ordered state at low-temperatures and high-pressures from neutron diffraction data.

II. EXPERIMENTAL METHOD

We have carried out time-of-flight neutron diffraction measurements at the Spallation Neutrons and Pressure (SNAP) beamline BL-3 at the Spallation Neutron Source (SNS), Oak Ridge National Laboratory. Pressure for these experiments was generated by a custom made diamond anvil cell (DAC) device with a large opening angle of 70^{o} x 120^{o} for neutron diffraction studies. The diamond anvils utilized in the experiments were chemical vapor deposition grown diamonds with a culet diameter of 2.1 mm [11,12]. A stainless-steel gasket (annealed 15-5 precipitation hardened) with an initial thickness of 1.2 mm was pre-indented to 440 µm with a set of WC dies in a hydraulic press, followed by a final forming step, using the DAC itself, to a final thickness of 185 µm. A gasket hole of 1 mm in diameter was drilled, and the gasket was heat treated in air at 500 ^{o}C for an hour to achieve full hardness (~46 Rockwell C). The sample chamber was filled with pieces cut from a commercial Dy foil (99.99% purity). A hexagonal boron-nitride incident beam collimation with a 0.5 mm diameter hole was placed in the upstream seat to narrow the beam and effectively reduce the background. The cell was attached to a closed-cycle refrigerator and lowered into a vacuum chamber such that the incident beam was coincident with the thrust axis of the pressure cell (i.e., the incident beam travels through the diamond anvils and the sample). The two detector banks, each covering ±22^o 2θ, were centered at 65^o and 90^o 2θ. The wavelength range of the neutrons was between 0.5 Å to 3.7 Å. The data was background subtracted and normalized. For the purposes of determining the peak intensities, the data in each pressure set was background subtracted using the background from the lowest temperature spectrum at 8 K.

The pressures were calculated using the measured volume of Dy, as determined from the diffraction data, using parameters extracted from earlier high-pressure, low-temperature x-ray diffraction experiments fitted to a third-order Birch-Murnaghan equation of state [13].

$$P = \frac{3}{2}B_0\left[\left(\frac{V_0}{V}\right)^{\frac{7}{3}} - \left(\frac{V_0}{V}\right)^{\frac{5}{3}}\right]\left\{1 + \frac{3}{4}(B_0' - 4)\left[\left(\frac{V_0}{V}\right)^{\frac{2}{3}} - 1\right]\right\} \qquad (1)$$

We want to treat this neutron diffraction study independent of earlier x-ray diffraction study at high-pressure and low-temperature [7] and hence pressures were calculated using the low-temperature unit-cell volume measured in this study and the known information on the equation of state of Dy. The sample pressures at high-pressures and low-temperatures were calculated using bulk-modulus (B_0) = 36 GPa and the pressure derivative of bulk-modulus B_0' = 3.5 (from reference [1]) with V_0 being the ambient pressure volume at low-temperatures obtained from the present neutron diffraction data.

III. RESULTS AND DISCUSSION

Magnetic Transitions in the Hexagonal Close Packed Phase

Figure 1 shows magnetic ordering in the hexagonal close packed (*hcp*) phase of Dy at ambient pressure. At a temperature of 295 K, a paramagnetic phase is observed where the nuclear peaks (100), (002), (101), (110), (103), (112), and (004) from the *hcp* phase are clearly observed (Figure 1 (a)). The measured lattice parameters for the *hcp* phase of Dy at 295 K are *a* = 3.610±0.002 Å, *c* = 5.671±0.002 Å with axial ratio *c/a* = 1.57. The Laue spot from single crystal diamond (D) and diffraction from hexagonal boron-nitride (h-BN) collimator, and steel gasket (G) are also labelled. On cooling below antiferromagnetic (AFM) transition temperature of 176 K, magnetic ordering is observed as evidenced by several magnetic superlattice reflections indicated by “M” at 150 K in Figure 1 (b). On further cooing to 50 K and ambient pressure, magnetic reflections corresponding to AFM phase disappears and a general enhancement of intensities of *hcp* nuclear peaks is observed. We measured an intensity enhancement of 28% in the (101) peak between 150 K and 50 K, indicating a ferromagnetic transition in Figure 1 (c).

Figure 2 shows magnetic ordering in Dy at a pressure of 4.6 GPa as revealed by neutron diffraction. At 200 K in Figure 2 (a), Dy is paramagnetic with nuclear peaks indexed to lattice parameters a = 3.481±0.002 Å, c = 5.471±0.002 Å with axial ratio c/a = 1.571 for the *hcp* phase at a pressure of 4.6 GPa. At a temperature of 125 K, AFM ordering is observed with additional superlattice reflections marked by "M" in Figure 2 (b). The AFM phase is stable up to 50 K at 4.6 GPa as shown in Figure 2(c) indicating that ferromagnetic transition has moved to below 50 K at this pressure.

Incommensurate Antiferromagnetic Phase and Helical Turn Angle:

The AFM transition in Dy can be described by a helical structure where the moments are aligned in the hexagonal basal plane and change their orientation from one hexagonal layer to the next given by a turn angle θ. The helical AFM magnetic structure can be described as an incommensurate phase as follows below where bold face notation is used for vectors.

The Bragg condition is that $\mathbf{\Delta K} = \mathbf{G}_{hkl}$ and $d_{hkl} = 2\pi/|\,\mathbf{G}_{hkl}\,|$ (2)

Where $\mathbf{\Delta K}$ is the change in wave vector and $\mathbf{G}_{hkl}$ is a reciprocal lattice vector and d_{hkl} is the interplanar spacing. $\mathbf{G}_{hkl}$ is given in terms of reciprocal lattice vectors $\mathbf{a}^*$, $\mathbf{b}^*$, and $\mathbf{c}^*$ and (*hkl*) are Miller indices

$$\mathbf{G}_{hkl} = \mathrm{h}\,\mathbf{a}^* + \mathrm{k}\,\mathbf{b}^* + \mathrm{l}\,\mathbf{c}^* \qquad (3)$$

The magnetic peaks "M" in the AFM phase are described by $\mathbf{\Delta K} = \mathbf{G}_{hkl} \pm \mathbf{q} = \mathbf{G}'$ (4)

The incommensurate wave vector $\mathbf{q} = \mathbf{c}^*/n$ where n is a non-integer (5)

The turn angle θ (in degrees) = $180/n$ (6)

The turn angle as described above is obtained from the experimental data and is plotted in Figure 4 as a function of temperature at ambient pressure and at a pressure of 4.6 GPa. The measured turn angle increases with increasing temperature at ambient pressure (0.14 degree/K) consistent with the earlier published results [8,9] where turn angle changed from 26.5 degree to 43.2 degree between 85 K and 179 K. On increasing pressure to 4.6 GPa, while the turn angle is larger, its temperature variation is not as steep (0.05 degree/K) as compared to ambient pressure.

Magnetic Ordering in the Alpha-Samarium (*α-Sm*) phase:

The origin of magnetic ordering in the high-pressure *α-Sm* phase in Dy remains unclear as earlier magnetic susceptibility measurements indicated loss of signal in the background and no magnetic transition was observed above 7.4 GPa [14]. The electrical transport measurements do indicate a magnetic ordering transition in Dy in the *α-Sm* phase above 7 GPa, however, whether the transition is AFM or FM in nature remains unclear. We did not observe any superlattice reflections at 10.8 GPa in the *α-Sm* phase in Dy during cooling from 200 K to 20 K. Figure 4 shows the neutron diffraction pattern at 10.8 GPa at various temperatures in the *α-Sm* phase and no additional magnetic super-lattice reflections are observed eliminating the possibility of AFM ordering. The measured lattice parameters for the *α-Sm* at 10.8 GPa and 20 K are a = 3.341±0.015 Å, c = 24.455±0.015 Å with axial ratio c/a = 7.29. In agreement with the absence of super-lattice reflections at 10.8 GPa, we do observe an enhancement of intensities of nuclear peaks with decreasing temperature indicating ferromagnetic ordering as illustrated for the (105) nuclear peak in Figure 4. The ferromagnetic transition temperature (T_C) is determined by neutron diffraction to be 59 K at a pressure of 10.8 GPa as indicated by an increase in intensity of the (105) nuclear peak in Figure 5. This observation is in close agreement with the T_C ~ 60 K reported in electrical transport measurements at high-pressure and low-temperature at 11 GPa [3, 4]. It should be added that the intensity enhancement of (105) nuclear peak reported in Figure 5 is below 10 % which is a small value for the ferromagnetic contribution of Dy atoms with a large magnetic moment of 10.6 μB. Therefore, it is concluded that we are observing an inhomogeneous magnetic state in Dy with magnetically ordered ferromagnetic domains coexisting within a paramagnetic state in the *α-Sm* phase at 10.8 GPa.

Negative Thermal Expansion in Dy at High Pressures:

The anomalous thermal expansion in single crystal Dy at low-temperatures and ambient pressure has been well documented [15]. Also, synchrotron x-ray diffraction studies on Dy at high pressures and low temperatures have suggested a near-zero thermal expansion for ambient and high pressure phases in the magnetically ordered regime [7]. Now that we have documented magnetic ordering transitions in Dy at high pressures by neutron diffraction, we look closely at the pressure and temperature dependence of the atomic volume. Figure 7 shows the measured atomic volume for Dy as a function of temperature at ambient pressure, 4.6 GPa, 7.7 GPa, and 10.8 GPa respectively. The data in Figure 7 has been plotted as a normalized change in volume ($\Delta V/V_0$) as a function of temperature where ΔV is the change in volume ($V-V_0$) and V_0 is the atomic volume at 200 K at various pressures. We observe an overall trend of increasing atomic volume with decreasing temperature or a negative thermal expansion in the magnetically ordered phases at all pressures. The volume increases by as much as 2.5% between 200 K and 8 K at a pressure of 7.7 GPa. The measured volume thermal expansion coefficient at 50 K is $-7.8*10^{-5}$ K^{-1} at 4.6 GPa and is $-2.34*10^{-4}$ K^{-1} at 7.7 GPa. The increase in volume on cooling correlates with the magnetic ordering at low temperature for each pressure as is shown in Figure 6. The thermal expansion is indeed anisotropic and anomalous as indicated by the plot of relative change in *a*-axis and *c*-axis on cooling from 200 K at 10.8 GPa as shown in Figure 7. The measured *c*-axis expands on cooling below 60 K while the measured *a*-axis contracts on cooling in the magnetically ordered state of *α-Sm* phase of Dy at 10.8 GPa. It is important to note that the ferromagnetic transition temperature of 60 K at 10.8 GPa determined from anisotropy in thermal expansion is in good agreement with the 59 K value determined from the enhancement of nuclear peaks shown in Figure 5.

IV. CONCLUSION

We have carried out neutron diffraction studies on rare earth metal Dysprosium (Dy) to 10.8 GPa and 8 K using a large-volume diamond anvil cell at the Spallation Neutron Source, Oak Ridge National laboratory. The antiferromagnetic and ferromagnetic ordering transitions are observed for the hexagonal close packed phase of Dy below 7 GPa. The incommensurate wave vector associated with antiferromagnetic transition shows rapid changes with both temperature and pressure resulting in a helical turn angle in the *hcp* phase that increases rapidly with increasing temperature as well as with increasing pressure. The long-standing issue of magnetic ordering in the high-pressure phases of rare-earth metal Dy is resolved by our neutron diffraction studies as only ferromagnetic phase transition is observed for the high pressure *α-Sm* phase. The ferromagnetic transition temperatures measured by neutron diffraction are in excellent agreement with the results from the electrical transport studies. The atomic volume measurements at various temperatures and pressures show the phenomenon of negative thermal expansion in the magnetically ordered phases of rare-earth metal Dy at all pressures. We observed an increase in volume of as much as 2.5% on cooling from 200 K to 8 K at a pressure of 7.7 GPa. It would be instructive to extend these studies to pressure beyond 70 GPa where electrical transport measurements indicate magnetic ordering approaching room temperature.

ACKNOWLEDGEMENTS

This material is based upon work supported by the Department of Energy-National Nuclear Security Administration under Award Number DE-NA0003916. A portion of this research used resources at the Spallation Neutron Source, a DOE Office of Science User Facility operated by the Oak Ridge National Laboratory.

REFERENCES

1. Gopi K. Samudrala, and Yogesh K. Vohra, “Structural Properties of Lanthanides at Ultra High Pressure” in Handbook on the Physics and Chemistry of Rare Earths, Jean-Claude G. Bünzli and Vitalij K. Pecharsky editors, Vol. 43, Elsevier, 2013, pp. 275-319.
2. Yogesh K. Vohra and Jagannadham Akella, "5-f bonding in thorium metal at extreme compressions: Phase Transitions to 300 GPa", Phys. Rev. Lett. **67**, 3563-3566 (1991).
3. Gopi K. Samudrala, Georgiy M. Tsoi, Samuel T. Weir & Yogesh K. Vohra, “Magnetic ordering temperatures in rare earth metal dysprosium under ultrahigh pressures”, High Pressure Research 34, 266-272 (2014).
4. J. Lim, G. Fabbris, D. Haskel, and J.S. Schilling, “Magnetic ordering at anomalously high temperatures in Dy at extreme pressures, Phys. Rev. B 91, 045116 (2015).
5. Thomas SA, Tsoi GM, Wenger LE, Vohra YK. “Magnetic and structural phase transitions in erbium at low temperatures and high pressures” Phys Rev B. 84 144415 (2011).
6. Sarah A. Thomas, Jeffrey M. Montgomery, Georgiy M. Tsoi, Yogesh K. Vohra, Gary N. Chesnut, Samuel T. Weir, Christopher A. Tulk & Antonio M. dos Santos. “Neutron diffraction and electrical transport studies on magnetic ordering in terbium at high pressures and low temperatures” High Pressure Research **33**, 555-562 (2013).
7. Kevin M. Hope, Gopi K. Samudrala, and Yogesh K. Vohra, “Near-zero thermal expansion in magnetically ordered state in dysprosium at high pressures and low temperatures”, Cogent Physics **4**, 1412107 (2017).
8. S. Legvold, F.H. Spedding, F. Barson, and J. F. Elliot, “Some Magnetic and Electrical Properties of Gadolinium, Dysprosium, and Erbium Metals” Reviews of Modern Physics **25**, 129-130 (1953).
9. R. D. Greenough, G. N. Blackie, and S. B. Palmer, “Commensurate turn angle effects in single-crystal antiferromagnetic dysprosium” J. Phys. C: Solid State Phys., **14**, 9-19 (1981).
10. M. K. Wilkinson, W. C. Koehler, E. O. Wollan, and J. W. Cable, “Neutron diffraction investigation of magnetic ordering in Dysprosium”, Journal of Applied Physics **32**, S48-S49 (1961).

11. R. Boehler, M. Guthrie, J. J. Molaison, A.M. dos Santos, S. Sinogeikin, S. Machida, N. Pradhan, and C. A. Tulk, "Large-volume diamond cells for neutron diffraction above 90 GPa", High Pressure Research **33**, 546-554 (2013).
12. R. Boehler, J. J. Molaison, and B. Haberl, "Novel diamond cells for neutron diffraction using multi-carat CVD anvils", Review of Scientific Instruments **88**, 083905 (2017).
13. F. Birch, "Finite Elastic Strain of Cubic Crystals" Phys. Rev. **71**, 809-824 (1947).
14. D. D. Jackson, V. Malba, S. T. Weir, P. A. Baker, and Y. K. Vohra, "High Pressure Magnetic Susceptibility Experiments on the Heavy Lanthanides Gd, Tb, Dy, Ho, Er, and Tm", Phys. Rev. **B 71**, 184416 (2005).
15. A. E. Clark, B. F. DeSavage, and R. Bozorth, "Anomalous Thermal Expansion and Magnetostriction of Single-Crystal Dysprosium", Phys. Rev. **138**, A216-A224 (1965).
16. E. B. Amitin, V.G. Bessergenev, and Y. A. Kovalevskaya, "Thermal expansion anomalies in dysprosium", J. Phys. F: Met. Phys. **14** 2935-2942 (1984).

FIGURE CAPTIONS

Figure 1: The back-ground subtracted neutron diffraction patterns for the *hcp* phase of Dy at ambient pressure (0.1MPa) and at various temperatures (a) in paramagnetic phase at 295 K, (b) Antiferromagnetic phase at 150 K (magnetic superlattice reflections indicated by "M"), and (c) Ferromagnetic phase at 50 K. The Laue spot from single crystal diamond (D) and diffraction from hexagonal boron-nitride (h-BN) collimator, and steel gasket (G) are also indicated.

Figure 2: The background subtracted neutron diffraction patterns for the *hcp* phase of Dy at high pressure of 4.6 GPa and at various temperatures (a) in paramagnetic phase at 200 K, (b) Antiferromagnetic phase at 125 K with several magnetic superlattice reflections indicated by "M", and (c) Antiferromagnetic phase at 50 K. The Laue spot from single crystal diamond (D) and diffraction from hexagonal boron-nitride (h-BN) collimator, and steel gasket (G) are also indicated.

Figure 3: The experimentally measured turn angle (θ) for the incommensurate antiferromagnetic phase in hexagonal close packed Dy at various pressures and temperatures. The linear fits to data at ambient pressure and at 4.6 GPa are described in the text.

Figure 4: The background subtracted neutron diffraction pattern in the high-pressure *α-Sm* phase at 10.8 GPa and at various temperatures down to 20 K. The measured lattice parameters for the sample are described in the text. No additional magnetic super-lattice reflections indicating antiferromagnetic magnetic ordering was observed to the lowest temperature. The nuclear peaks show enhancement in intensities on cooling indicating the onset of ferromagnetic state.

Figure 5: The integrated intensity of (105) nuclear diffraction peak of the *α-Sm* phase of Dy with temperature between 8 K and 200 K at a pressure of 10.8 GPa. The increase in intensity at 59 K signals magnetic phase transition to a ferromagnetic state.

Figure 6: The measured normalized change in atomic volume ($\Delta V/V_0$) for Dy at various pressures and temperatures by neutron diffraction. There is an overall trend of increasing atomic volume with decreasing temperature or a negative thermal expansion in magnetically ordered phases at all pressures.

<u>Figure 7</u>: The measured change in lattice parameters in the *α-Sm* phase of Dy as a function of temperature on cooling from 200 K at a pressure of 10.8 GPa. The anisotropic and anomalous behavior between the *a*-axis and the *c*-axis is clearly apparent at low temperatures below 60 K in the magnetically ordered phase.

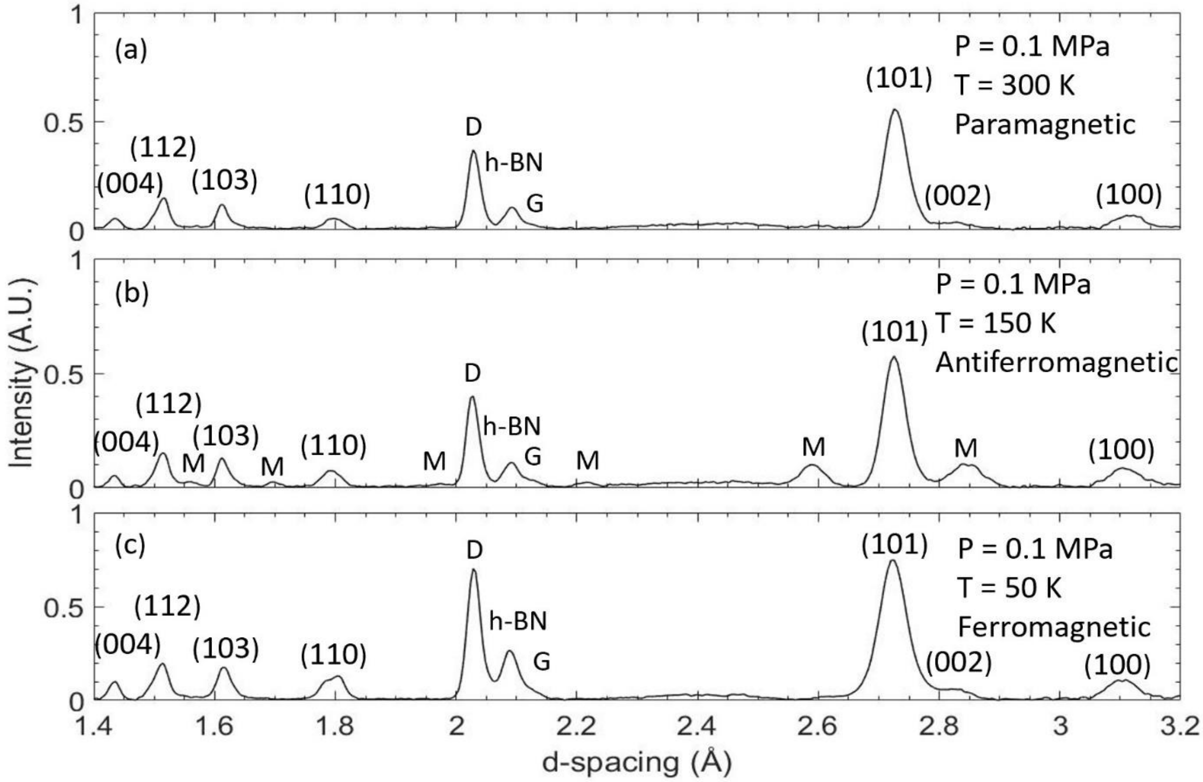
(a)
P = 0.1 MPa
T = 300 K
Paramagnetic
(101)
(112)
(004)
(103)
(110)
D
h-BN
G
(002)
(100)
(b)
P = 0.1 MPa
T = 150 K
Antiferromagnetic
(101)
(112)
(004)
(103)
(110)
M
M
M
D
h-BN
G
M
M
M
(100)
(c)
P = 0.1 MPa
T = 50 K
Ferromagnetic
(101)
(112)
(004)
(103)
(110)
D
h-BN
G
(002)
(100)
Intensity (A.U.)
d-spacing (Å)
0
0.5
1
1.4
1.6
1.8
2
2.2
2.4
2.6
2.8
3
3.2

FIGURE 1

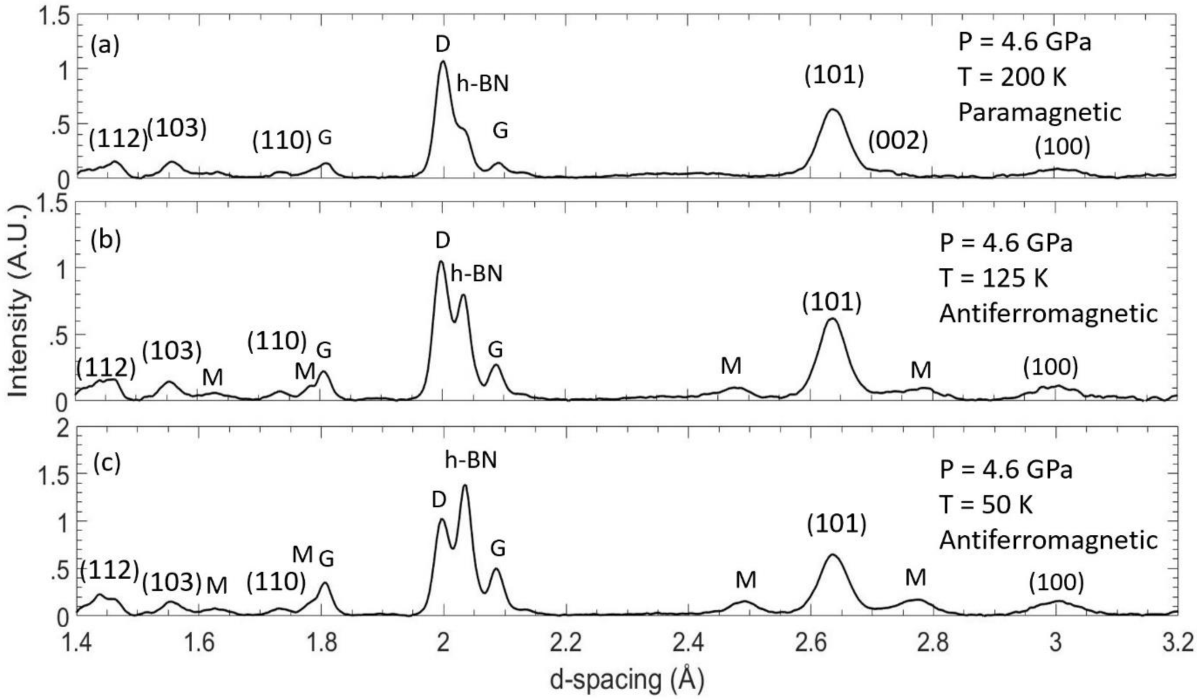
(a)
D
h-BN
G
(112)
(103)
(110)
G
(101)
(002)
(100)
P = 4.6 GPa
T = 200 K
Paramagnetic
(b)
D
h-BN
G
(112)
(103)
M
(110)
M
G
M
(101)
M
(100)
P = 4.6 GPa
T = 125 K
Antiferromagnetic
(c)
h-BN
D
G
(112)
(103)
M
(110)
M
G
M
(101)
M
(100)
P = 4.6 GPa
T = 50 K
Antiferromagnetic
Intensity (A.U.)
d-spacing (Å)

FIGURE 2

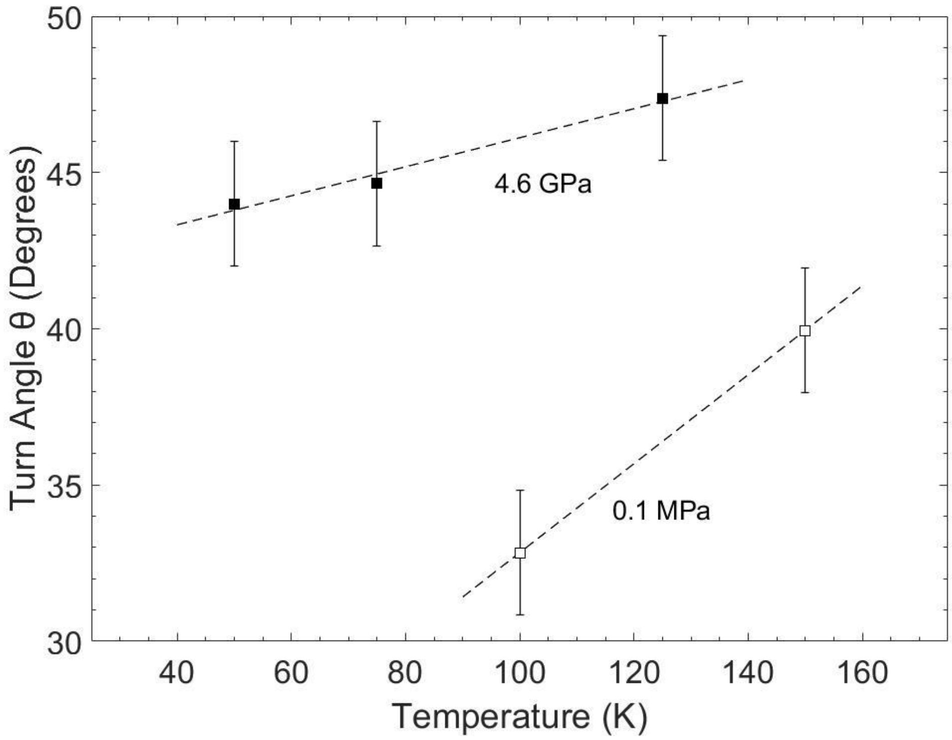
50
45
40
35
30
Turn Angle θ (Degrees)
40
60
80
100
120
140
160
Temperature (K)
4.6 GPa
0.1 MPa

FIGURE 3

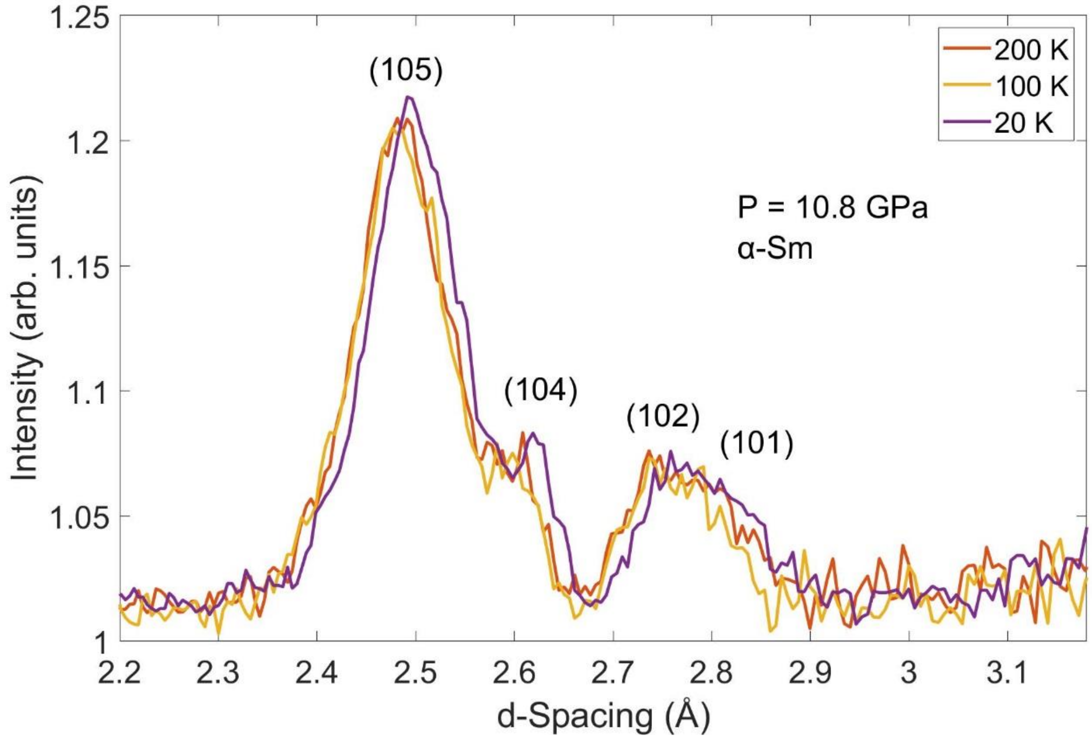

1.25
1.2
1.15
1.1
1.05
1
Intensity (arb. units)
2.2
2.3
2.4
2.5
2.6
2.7
2.8
2.9
3
3.1
d-Spacing (Å)
200 K
100 K
20 K
(105)
(104)
(102)
(101)
P = 10.8 GPa
α-Sm

FIGURE 4

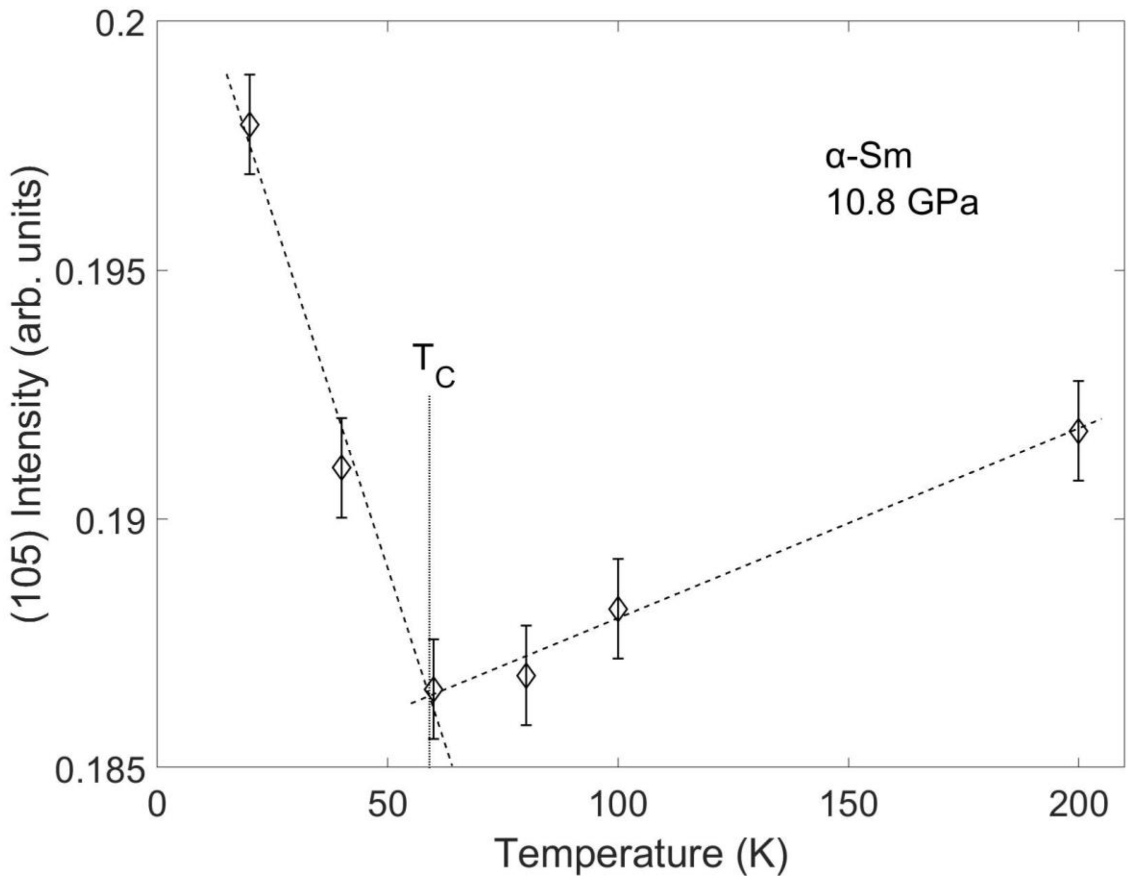
α-Sm
10.8 GPa
T_C
(105) Intensity (arb. units)
Temperature (K)
0.2
0.195
0.19
0.185
0
50
100
150
200

FIGURE 5

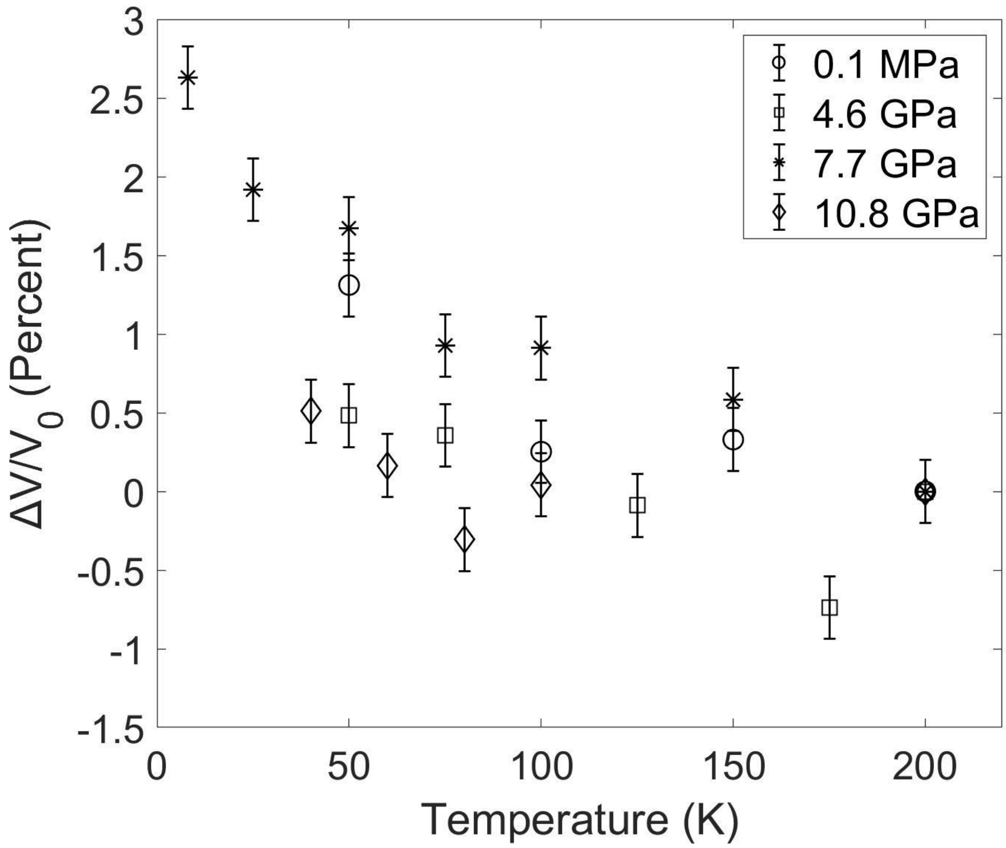
0.1 MPa
4.6 GPa
7.7 GPa
10.8 GPa
$\Delta V/V_0$ (Percent)
Temperature (K)
3
2.5
2
1.5
1
0.5
0
-0.5
-1
-1.5
0
50
100
150
200

FIGURE 6

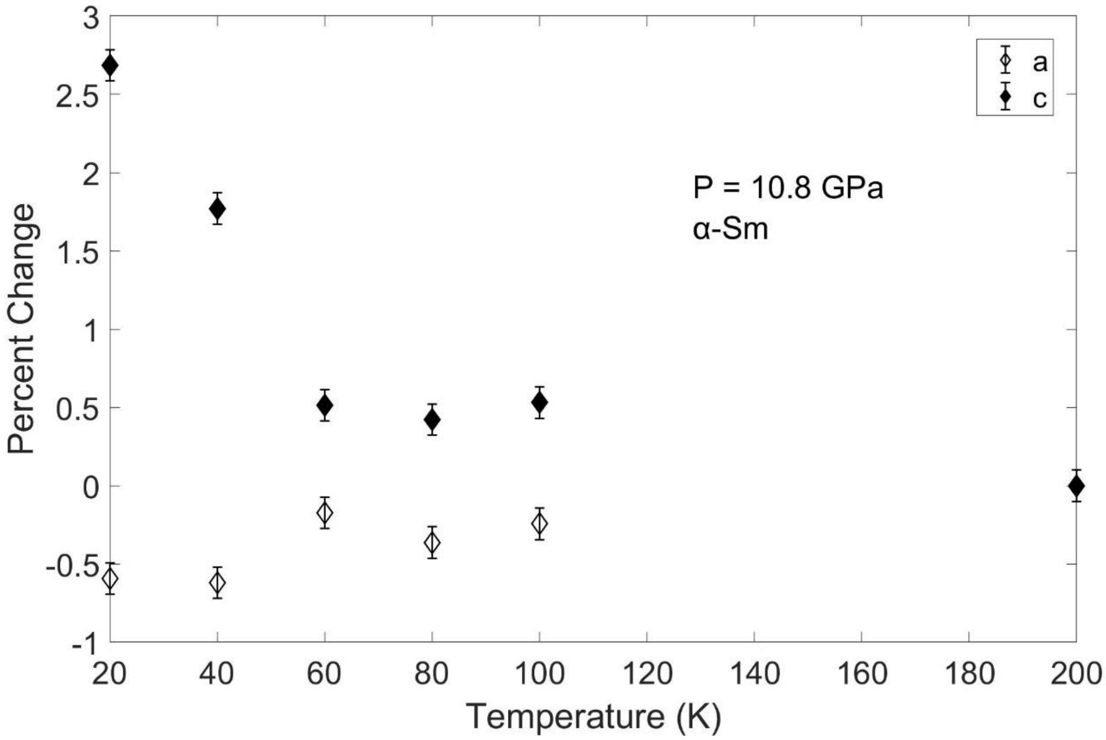
P = 10.8 GPa
α-Sm
a
c
Percent Change
Temperature (K)
3
2.5
2
1.5
1
0.5
0
-0.5
-1
20
40
60
80
100
120
140
160
180
200

FIGURE 7